REPORT DOCUMENTATION PAGE

Form Approved
OMB No. 0704-0188

1. AGENCY USE ONLY (Leave blank)	2. REPORT DATE	3. REPORT TYPE AND DATES COVERED
	July 29, 1995	Technical Report / June 1994-May 1995

4. TITLE AND SUBTITLE
Measurements of the Potential Dependence of Electric Field Magnitudes at an Electrode Surface Using Fluorescent Probes in a Self-Assembled Monolayer

5. FUNDING NUMBERS
Grant # N00014-90-J-1167

R&T Code 4133019

6. AUTHOR(S)
John Pope and Daniel Buttry

7. PERFORMING ORGANIZATION NAME(S) AND ADDRESS(ES)
Department of Chemistry, University of Wyoming
Laramie, WY 82071-3838

8. PERFORMING ORGANIZATION REPORT NUMBER

9. SPONSORING/MONITORING AGENCY NAME(S) AND ADDRESS(ES)
Office of Naval Research
Chemistry Division
800 N. Quincy Street
Arlington, VA

10. SPONSORING/MONITORING AGENCY REPORT NUMBER
Technical Report
#25

11. SUPPLEMENTARY NOTES
Prepared for publication in Journal of the American Chemical Society

12a. DISTRIBUTION/AVAILABILITY STATEMENT
This document has been approved for public release and sale; its distribution is unlimited

12b. DISTRIBUTION CODE

13. ABSTRACT *(Maximum 200 words)*

Abstract - This report details the measurement of the dependence of the electric field magnitude on applied potential in two regions of the electrical double layer, inside the Outer Helmholtz Plane (OHP), i.e. inside the monolayer, and in the diffuse layer, for a metal/organic thin film/electrolyte system. The self-assembled monolayers (SAM's) used in these experiments were formed from n-alkyl thiols on roughened Ag and roughened or smooth Au electrodes. The electric field magnitudes were calculated from the Stark shifts of a cationic fluorescent probe, an (aminostyryl)pyridinium derivative, that was immobilized in the SAM. The chain lengths of these alkyl thiols were varied to control the distance of the probe from the OHP and thus the relative position of the probe in the electrical double layer. Two cases were examined, one in which the probe was embedded within the SAM, and another in which the probe was external to the SAM. The composition of the monolayers and the orientation of the probe and n-alkyl thiol molecules within them were characterized using *ex situ* reflection-absorption Fourier transform infrared spectroscopy (RA-FTIR). For the case in which the probe was embedded within the SAM, the electric field magnitude was determined to be 3×10^5 V/cm per volt of applied potential, while for the case of the probe outside of the SAM a value of 4×10^4 V/cm per volt of applied potential was obtained. These values are smaller than expectations based on existing models for the potential distributions within such structures, and possible reasons for this behavior are discussed. A potential dependence of the fluorescence intensity of the probe was also observed.

14. SUBJECT TERMS
electrochemistry, electric field, monolayer

15. NUMBER OF PAGES
32

16. PRICE CODE

17. SECURITY CLASSIFICATION OF REPORT	18. SECURITY CLASSIFICATION OF THIS PAGE	19. SECURITY CLASSIFICATION OF ABSTRACT	20. LIMITATION OF ABSTRACT
unclassified	unclassified	unclassified	UL

OFFICE OF NAVAL RESEARCH

GRANT #: N00014-90-J-1167

R&T Code: 4133019

Technical Report No. 25

Measurements of the Potential Dependence of Electric Field Magnitudes at an Electrode Using Fluorescent Probes in a Self-Assembled Monolayer

John M. Pope and Daniel A. Buttry

Prepared for publication

in

Journal of the American Chemical Society.

Department of Chemistry
University of Wyoming
Laramie, WY 82071-3838

July 29, 1995

Measurements of the Potential Dependence of Electric Field Magnitudes at an Electrode Using Fluorescent Probes in a Self-Assembled Monolayer

John M. Pope and Daniel A. Buttry*

Department of Chemistry

University of Wyoming

Laramie, WY 82071-3838

Abstract - This report details the measurement of the dependence of the electric field magnitude on applied potential in two regions of the electrical double layer, inside the Outer Helmholtz Plane (OHP), i.e. inside the monolayer, and in the diffuse layer, for a metal/organic thin film/electrolyte system. The self-assembled monolayers (SAM's) used in these experiments were formed from n-alkyl thiols on roughened Ag and roughened or smooth Au electrodes. The electric field magnitudes were calculated from the Stark shifts of a cationic fluorescent probe, an (aminostyryl)pyridinium derivative, that was immobilized in the SAM. The chain lengths of these alkyl thiols were varied to control the distance of the probe from the OHP and thus the relative position of the probe in the electrical double layer. Two cases were examined, one in which the probe was embedded within the SAM, and another in which the probe was external to the SAM. The composition of the monolayers and the orientation of the probe and n-alkyl thiol molecules within them were characterized using *ex situ* reflection-absorption Fourier transform infrared spectroscopy (RA-FTIR). For the case in which the probe was embedded within the SAM, the electric field magnitude was determined to be 3×10^5 V/cm per volt of applied potential, while for the case of the probe outside of the SAM a value of 4×10^4 V/cm per volt of applied potential was obtained. These values are smaller than expectations based on existing models for the potential distributions within such structures, and possible reasons for this behavior are discussed. A potential dependence of the fluorescence intensity of the probe was also observed.

Introduction

The spontaneous adsorption of molecules at surfaces represents a simple and powerful method of constructing interfaces with well-defined structure and composition.[1] In particular, the use of thiol- or disulfide-bearing species to form self-assembled monolayers (SAM's) at various metal surfaces has proven to be a very attractive method for investigating fundamental electrochemical phenomena related to the influence of surface structure on redox processes. Our group has been particularly interested in understanding how the interfacial environment in or near such structures might differ from the bulk, thereby inducing behavior that is unique compared to bulk behavior. For example, we have investigated how ion-pairing within SAM's[2] and the position of the redox group within a SAM[3] affects the electron transfer processes of such groups in SAM's. In addition, we have used the electrochemical quartz crystal

microbalance (EQCM) to study ion insertion and expulsion processes that are driven by changes in the charge of these redox groups.[2,3] These studies demonstrated that SAM's with redox groups whose state of charge can be electrochemically modulated behave as molecularly thin ion-exchange materials. To better understand the forces that drive these ion-exchange processes, we decided to investigate more closely the basic structure of the electrical double layer at such interfaces, which is the topic of this contribution.

The study of interfacial potential distributions has a long history, and several mathematical models have been developed to describe them.[4-6] While there have been many discussions of relatively indirect methods to estimate interfacial potential distributions, such as double layer electrode kinetic effects[5], there are surprisingly few direct measurements of interfacial electric field strengths or potential profiles[7-10]. We present here the results of a new experimental strategy for measurement of electric field strengths at solid-liquid interfaces that employs a surface-immobilized, oriented, fluorescent dye as a spectroscopic probe of the interfacial electric field. A preliminary report of this approach has been presented.[11] This technique has been used extensively to measure electric fields in biological membranes.[12,13] There are also a few previous reports of the use of optical spectroscopies to measure interfacial electric fields in electrochemical systems[14], but in those cases the π systems of the probe chromophores were in direct contact with the electrode surface, making it difficult to differentiate purely electrostatic effects from inductive effects.[14]

The present method, referred to as electrochromism[15] or the Stark effect[16], involves measuring a change in the electronic transition energy of the probe immobilized in the electrical double layer as the local electric field is perturbed.[16,17] The phenomenon that manifests as this change in energy involves an electrostatic interaction between both the ground and excited state dipoles of the probe and the local, interfacial electric field created by a potential drop that is applied across the double layer. This interaction is written mathematically[18] with an expression containing the scalar product of the vector describing the change in the dipole moment between the ground and excited states of the probe and the electric field vector (which is presumed to be normal to the surface[4-6]), as in equation 1,

$$h\Delta\nu = -\Delta\mu\,\Delta E\cos\theta - 1/2\,\Delta\alpha_{ge}\,\Delta E^2\cos\theta \qquad (1)$$

where h is the Planck constant, $\Delta\nu$ is the shift in energy of the peak between any two electric fields (i.e. at any two applied potentials), $\Delta\mu$ is the total change in dipole moment between the ground and excited states of the dye (a constant particular to each probe molecule), ΔE is the change in the magnitude of the electric field between any two applied potentials, θ is the angle between the vectors, and $\Delta\alpha_{ge}$ is the change in the polarizability between the ground and excited states. The quadratic term arises from the change in the ground and excited state dipole moments due to the polarizabilities of these states, and is usually negligible for electric field magnitudes below ca. 10^7 V/cm.[18] It is important to note that, in the present context, this equation refers to the **change** in electric field between any two applied potentials. Knowledge of the absolute electric field at any applied potential requires knowledge of the potential at

which the electric field vanishes (i.e. the potential of zero charge or E_{pzc}), so that the Stark shift can be measured with respect to that potential. We return to a discussion of this point later.

Equation 1 shows that the Stark shift is linear in $\Delta\mu$. Thus, chromophores with large changes in dipole moment during excitation or emission should exhibit the largest Stark shifts. This property is commonly observed for donor-acceptor compounds of the type exemplified by the hemicyanine derivative used here (Scheme 1). In fact, the choice of the hemicyanine probe for the present study was based in part on extensive computational[18a] examination of $\Delta\mu$ for a variety of candidate probes, most of which comprised donor-acceptor systems, as well as an experimental investigation of $\Delta\mu$ for the hemicyanine derivative.[18b] Another consideration in the choice of the hemicyanine probe was the availability of a relatively tractable synthetic route to the thiol derivative required for its immobilization within the SAM. However, as will become clear below, the choice of a cationic probe molecule is not without its drawbacks. Finally, the photophysical characteristics of the probe are very important in determining its suitability for these experiments (vide infra).

The above mathematical expression has several experimental ramifications, the most obvious of which is that the dipole moments and electric field have a maximum interaction, and thus a maximum measurable Stark shift, when their vectors are parallel, i.e. when the transition moment of the dye's intramolecular charge-transfer transition is perpendicular to the metal surface. We have satisfied this physical condition by employing steric constraints through judicious choice of alkanethiol "filler" molecules. Thus, the probe molecules are embedded within monolayers of n-alkyl thiols whose lengths were chosen to promote a parallel orientation of the long-axis of the dye with respect to the surface normal. As discussed below, this orientation has been determined through the use of reflection-absorption Fourier transform infrared spectroscopy (RA-FTIR).

The interaction between the electric field and the probe's ground and excited state dipole moments manifests itself in both the absorption and emission processes, so, in principle, either could be used to measure the Stark shift. The previous electrochemical application of this type of measurement employed the absorption process.[14] We have chosen to use the emission process because it is intrinsically a much more sensitive experimental method than is absorption spectroscopy. However, emission of molecules near metal surfaces is greatly influenced by the metal, so several important considerations enter into the choice of appropriate compounds and conditions for such experiments. Fluorescence of molecules near metal surfaces has been shown to be strongly quenched by energy transfer to the metal surface,[19,20] although under the proper conditions fluorescence can occur[19, 21] and can even be enhanced.[22-24] Typically, this quenching leads to dramatically shorter fluorescence lifetimes and intensities than would otherwise be observed. However, recent work by Corn and coworkers,[25] as well as the results reported here, clearly show that it is possible to observe fluorescence from molecules situated at a metal surface, so long as the chromophoric part of the molecule is not in direct contact with the metal. It is worth noting

that a primary function of the n-alkyl thiol component of the SAM's used here is to prevent such direct contact so as to allow for observable emission intensity from the probe.

The detailed kinetic situation expected for an emitter near a semiconductor[26,27] or metal[27] surface has been described, and it is instructive to consider it in the context of the present discussion. The intrinsic lifetime for an emitter in bulk solution, τ_{obs}, is related in the following way to the rate constants for its radiative, k_r, and non-radiative, k_{nr}, processes:

$$1/\tau_{obs} = k_r + k_{nr} \qquad (2)$$

When placed near a metal, two new decay processes become possible. These are electron transfer between the excited state and the surface (actually, there may be two such rate constants that are relevant, one for reduction and one for oxidation of the excited state) and energy transfer to the surface, with rate constants k_s and k_{ET}, respectively. Thus, the lifetime expression must be modified in the following way:

$$1/\tau_{obs}' = k_r + k_{nr} + k_s + k_{ET} \qquad (3)$$

Equation 3 makes it clear that the ability to observe fluorescence from a species near a metal surface depends critically on the relationship between the rate constants for the emission process and the various decay processes. Specifically, the ability to observe reasonable emission intensity from the emitter requires that the intrinsic lifetime be very short so that the radiative process can compete effectively with the electron and energy transfer processes. Thus, a short intrinsic lifetime is seen to be an important criterion in choosing a probe molecule for studies of this type. In the present case, the lifetime of the probe is estimated to be ca. 100 ps based on a previous study of the lifetimes of several very similar derivatives in a variety of solvents[28]. This gives a value for $1/\tau_{obs}$ of ca. 10^{10} s^{-1}. This is quite fast, so that emission is expected to be competitive with the two interfacial quenching processes, which is, indeed, the case as will be seen below.

A recent, lucid model of the potential distribution at the metal/monolayer/electrolyte interface predicts large, linear potential drops across the monolayer followed by smaller decays into the diffuse layer.[6] To test the predictions of this model, we have examined the potential dependence of the Stark shifts of the probe in two types of experiments. In one, the probe is embedded within the alkyl chain region of the SAM, and in the other it extends into the diffuse part of the double layer. In both cases, the ionic strength, and thus the Debye length of the diffuse layer, are held constant.

Experimental

The field dye was synthesized according to a published route[29], although conversion of the hemicyanine (Figure 1a) to the bromide derivative (Figure 1b) and subsequently to the thiol (Figure 1c) was carried out by an approach described here. Hemicyanine was dissolved in hot toluene (EM Omnisolv) and 1,3-dibromopropane (Aldrich, 12,590-3) was added in a 5 equivalent excess. The reaction was catalyzed by 1% equivalent of tetrabutylammonium iodide (Aldrich, 14,077-5). The quaternized nitrogen

product precipitated as a red solid, which was filtered and washed with toluene and diethyl ether (Mallinckrodt Analytical Reagent) (60% yield) [^{1}H NMR (270 MHz) δ 4.5 (t, 2 H), 3.6 (t, 2 H), 3.0 (s, 6 H)]. To make the thiol functionality, an equivalent of Cs_2CO_3 (Aldrich, 20,212-6) was dissolved in absolute methanol (Baker Analyzed Reagent). An equivalent of thiolacetic acid was added to the solution to form the thioacetate anion nucleophile. A concentrated methanolic solution of dye in the 3 carbon chain/bromide form (referred to as the 1PAS3Br form) was added, and the resulting solution was refluxed under N_2 for ca. 24 hours. The solution was evaporated to dryness to obtain the thioester [^{1}H NMR (270 MHz) δ 4.5 (t, 2 H), 3.0 (s, 6 H), 2.9 (t, 2 H), 2.35 (s, 3 H), 2.15 (p, 2 H)], which was cleaved to the thiol by published procedures.[30] The resultant product was precipitated from a methanol/sat. $NaNO_3$ water mixture as the nitrate salt. Note that the procedure to convert the bromide to the thiol was used in place of previous preparations involving substitution of a halide by thiourea. We feel that cleavage of the thiourea to the thiol functionality under basic conditions provides an opportunity for oxidation of the thiol to the disulfide by adventitious oxygen which would have serious implications for the resultant structure of the monolayer.

Monolayers were immobilized on the metal electrodes described below by immersion of the prepared substrate in a solution with a total thiol concentration of 1 mM containing either a pure species (dye or n-alkyl thiol) or a mixture of species (dye + n-alkyl thiol) in abs. methanol for ca. 30 minutes. After loading, the samples were gently washed with copious amounts of methanol and deionized water and immediately placed in either an experimental cell or desiccator. Ratios of concentrations for loading solutions of mixed species were 1:10 for the dye:propanethiol solution and 1:1 for the dye:dodecanethiol solution. These ratios were chosen based on previous determination of the relative abilities of these alkanethiols to exclude the dye molecules from surface sites (see below).

Bulk FTIR spectra were taken in transmission a methanolic dye solution absorbed onto a microporous polyethylene disposable card (3M, KC-0061). The card was dried at 60° for 10 minutes prior to measurement, and the spectrum was ratioed against a clean card. 256 scans were taken at a resolution of 2 cm^{-1}.

For the FTIR monolayer orientation measurements, smooth Au substrates were prepared by depositing 75 Å of Cr and 2000 Å of Au on precleaned (NoChromix bath, GOORX Laboratories, Inc.) float glass 1x3 inch microscope slides (Fisher, 12550-A). Coating was performed via thermal evaporation using an Edwards 306A vapor deposition chamber and monitored with a quartz microbalance (Edwards, FTM4). Au deposition rate was ca. 1 Å per second. The resultant slides were placed directly into the loading solutions.

RA-FTIR spectroscopy measurements were done on a Bomem MB-100 FTIR spectrometer equipped with a narrow band, liquid nitrogen-cooled HgCdTe detector and a Harrick VRA glancing angle attachment with the reflection angle set at 80°. Spectra of the monolayer were ratioed against a

background of perdeuterated hexadecane thiol monolayer on smooth Au. Contributions to the spectra from atmospheric water and CO_2 were subtracted using the appropriate blanks. Spectra were obtained at 2 cm^{-1} resolution with 2048 co-added scans.

Rough Au substrates for the fluorescence measurements were initially prepared by mechanically polishing gold foil (Aldrich, 34,927-5, 99.99% pure, 0.05 mm thick) with 0.05 μm alumina grit (Buehler Micropolish B) and sonicating in deionized water for 15 minutes. Then, roughening[25] was done by electrochemically cycling the foil from -0.8 V to 1.9 V and back for two to three cycles in 0.1 M KCl. Rough Ag substrates were prepared as reported previously[11].

In situ fluorescence measurements were performed using a 90° excitation/collection geometry. For the monolayers on gold, the 4765 Å line of a Stabilite 2017 argon ion laser (Spectra-Physics) on power feedback control for stability was used as the excitation source. The beam was passed through a plasma line filter (Physical Optics) and focussed by a cylindrical lens onto the sample with an intensity of ca. 3 mW. The fluorescence was collected at 90° with a photographic lens (Nikolai Optics, f=2). A holographic notch filter (Kaiser Optical Company, Notch Plus) was used to reduce the collection of Rayleigh scattering. Spectra were obtained with a Spex 270M monochromator (0.27 m) equipped with an 1800 gr/mm holographic grating and a liquid nitrogen-cooled charge-coupled device detector (SpectrumOne, 256x1024 pixels). To obtain the multiple wavelength regions required for a complete fluorescence spectrum, spectra were obtained in 40 nm increments. Spectra of samples on Au substrates were obtained with an entrance slit width of 1 mm. Fluorescence spectra of samples on silver substrates were obtained as reported previously[11].

The applied potential in the fluorescence measurements was controlled by a poteniostat (Bioanalytical Systems, Inc., CV-1B-120). The electrochemical cell was a conventional glass H-cell. Voltages are reported versus a Ag/AgCl microreference (Bioanalytical Systems, MF 2063) with a Pt wire counter electrode. Ar gas was used to purge the cell of oxygen prior to all experiments.

Calculations of the ground state dipole moment and vibrational spectrum of the probe were done using the Spartan quantum chemistry package (Spartan SGI version 4.0.3, Wavefunction, Inc., Irvine, CA) at the AM1 level.

Results

RA-FTIR Characterization of the Monolayers

As mentioned above, two different monolayer structures were examined using the Stark shift experiment, one in which the probe was embedded within a monolayer of 12-carbon long n-alkyl chains and one in which the probe was pendent from the exterior of a monolayer of 3-carbon long n-alkyl chains. The mixed monolayers formed with these compositions are hereafter referred to as 1PAS3/C12 and 1PAS3/C3, respectively. In the 1PAS3/C12 case, the fact that the probe is surrounded by alkyl chains that

are of roughly the same length suggests that it should be held in an orientation in which the long axis of the probe is colinear with the long axis of the alkyl chains. In the 1PAS3/C3 case, there are at least two factors that could influence the orientation of the probe. First, molecular models suggest that unfavorable steric interactions between the ortho hydrogens of the pyridinium ring and the hydrogens of the terminal methyl groups of the propyl chains will occur if the probe tilts too far away from a perpendicular orientation (with respect to the plane of the surface). Second, at potentials negative of the E_{pzc} where the surface charge is negative, the perpendicular orientation of the probe is favored by electrostatics, because of a favorable interaction between the ground state dipole of the probe and the interfacial electric field. Changes in orientation due to the imposition of external electric fields have been observed for LB films containing dipolar species[31], although due to the restricted environment of the LB film, the small applied fields (ca. 1-5 kV/cm), and the small dipole moment of the dipolar species (ca. 0.1 D), these changes were limited to a few degrees change in the tilt angle (note that there are errors in the calculation of the electrostatic interaction energy in ref. 31). For our case, given that the E_{pzc} of Au is near +0.2 V[32], these orientational effects of the applied field should be strongest for applied potentials considerably negative of this value. In fact, for SAM's on Au substrates, most of our experiments were done with the applied potential negative of the E_{pzc} (for reasons that will be discussed below), where the electric field favors a perpendicular orientation.

These arguments suggest, but certainly do not prove, that the probe should take a perpendicular orientation in both types of SAM's, a conclusion that is supported by the RA-FTIR results presented below. The approximate geometry suggested by molecular models for the case of a probe with the orientation shown in Scheme 1 is that the pyridinium nitrogen of the acceptor ring system is 5 Å away from the surface, and the aniline nitrogen of the donor ring system is 15 Å from the surface. For the first type of monolayer the dodecylthiol chains should extend 16 Å from the surface, while for the second type the propylthiol chains should extend only 5 Å from the surface.

Because of its importance to the calculation of the electric field magnitude using equation 1, the orientation of the probe species in these two monolayers was investigated using RA-FTIR. Figures 2 and 3 show the spectra for a 1PAS3/C12 monolayer and for a bulk sample of the probe (structure c in Fig. 1). These spectra show the vibrational bands that are characteristic of the probe in the SAM, particularly the bands at 1640 cm^{-1} for the stretch of the vinylic C=C bond connecting the two rings, at 1164 cm^{-1} for the stretch of the C-N bond between the pyridinium nitrogen and the first methylene group in the propyl spacer of the probe molecule, and at 1583 cm^{-1}, which is a ring mode of the probe. The bands at 1640 cm^{-1} and 1164 cm^{-1} are of particular relevance, because they can be used to qualitatively evaluate the orientation of the probe species within the SAM, an issue to which we now turn.

The use of RA-FTIR spectra to determine orientations of adsorbates on metal surfaces has been described in considrable detail.[34,35] A rigorous, quantitative determination of orientation from such measurements requires detailed knowledge of the optical functions of the metal and adsorbate as functions

of frequency, and, even then, several assumptions must be made. Especially important is the assumption that the transition moments of the normal modes that result in the observed spectral bands can be quantitatively described, i.e. that their directionality with respect to the molecular axes can be determined. In the present case, this assumption is almost certainly not justified, because the modes that are readily identified in the RA-FTIR spectra are normal modes that contain contributions from various bonds in the two ring systems. To obviate the need for detailed knowledge of the optical functions of the substrate and adsorbate, we have opted for a simpler, qualitative evaluation of orientation based on a simple comparison of the ratios of the absorbances of two, non-parallel modes. In this method, changes in the relative absorption intensity ratios of vibrational bands in bulk and monolayer spectra are assumed to be entirely due to the anisotropy imposed on the optical electric field by the reflecting surface.[36] This assumption allows one to ignore variations in intensity between the bulk and monolayer spectra that are due to the different collection geometries by using a ratio of the intensities of two bands with known (or assumed) transition moment directions. The orientation of the probe in the monolayer is then obtained by iteratively projecting the vectors of these two modes with magnitudes equal to the ratio of intensities measured in the bulk spectrum onto the perpendicular electric field vector at varying orientations until the observed ratio of intensities in the monolayer spectrum is correctly predicted. This approach is conceptually identical to one recently described by Pemberton et al.[37] for the determination of the orientation of low symmetry molecules on metals using surface enhanced Raman scattering (SERS). Note that the analysis used here completely neglects contributions to the 1168 and 1640 cm^{-1} bands by any vibrations other than those of the C-N and C=C bonds, i.e. we are assuming that the transition moments for these two normal modes are directed along the stretching direction for these two bonds.

For a ratio of intensities in the bulk spectrum of ca. 5 (for the 1168 mode:1640 mode, which are geometrically separated by 54°[38]), this method correctly predicts the measured ratio of intensities in the monolayer spectrum of ca. 7.5 when the C-N bond (which is approximately parallel to the charge transfer axis of the probe) is -5° off normal with respect to the gold surface and the vinylic C=C mode is 49° off normal with respect to the gold surface. Thus, these RA-FTIR measurements qualitatively suggest that the long axis of the probe molecule, and therefore also the charge transfer axis for the intramolecular CT band, is approximately perpendicular to the plane of the surface. This orientation agrees with the odd-even effect of thiol adsorption on noble metals[39] which also predicts a tilt angle for the charge transfer axis of ca. 0° for the molecule adsorbed onto gold and ca. 60° for the molecule adsorbed onto silver. Finally, it is important to note that the Stark shift in equation 1 is a relatively weak function of θ for small values of θ (a tilt angle of as much as 60° from normal decreases the interaction energy by only 0.5). Thus, even though relatively poor assumptions have been made about the directions of the transition moments for the two normal modes used in the analysis, they are not likely to have a significant adverse impact on the quantitative calculation of electric field magnitudes from the Stark shifts.

Raman and Fluorescence Spectra of the Monolayers

Before proceeding with a discussion of the Stark shift measurements, it is worth briefly presently the results of an unsuccessful experiment, because it is instructive as to the spectroscopic characteristics that are indicative of problems with the monolayers that arise from their instability. A few monolayer samples were prepared from mixtures of the probe and 1-mercaptoethane (as opposed to 1-mercaptopropane) to give SAM's of the type 1PAS3/C2. As we have described previously[40], these short chain alkyl thiol SAM's are relatively unstable and desorb slowly when placed into aqueous solutions. Figure 4 shows the result of an attempt to obtain a fluorescence spectrum from such a sample on roughened Ag. While there is clearly a broad emission signature from the SAM, there are also prominent, sharp peaks in the spectrum. The positions of these at 1219 cm^{-1}, 1599 cm^{-1}, and several other values unambiguously identify them as due to SERS from adsorbed probe molecules[41]. We attribute this type of response as due to the desorption of a significant fraction of the 1-mercaptoethane component of the SAM, followed by *direct* adsorption of the π system of the probe onto the underlying Ag electrode surface. This causes nearly complete quenching of the emission of the probe, as well as the appearance of strong SERS peaks. This interpretation is in agreement with similar arguments recently made by Corn and coworkers regarding their observation of fluorescence from an adsorbed monolayer of methylene blue under conditions where direct access to the surface by the methylene blue was prevented by a layer of adsorbed sulfur.[25] These observations of the SERS response produced when the SAM framework that supports the probe at the surface is unstable are valuable inasmuch as they reveal the spectral signatures that define a poorly assembled monolayer. They also show the potency of the metal surface for quenching the probe emission and the very strong dependence of this quenching on the exact placement of the probe at the surface.

Figure 5 shows the *in situ* fluorescence spectrum obtained from a 1PAS3/C3 SAM on a roughened Au substrate (curve a), and a spectrum similarly obtained from a bare Au surface (curve b), both at open circuit conditions. Figure 6 gives the excitation and emission spectra for the probe dissolved in an aquous 0.1 M Na_2SO_4 solution, which shows the strong emission band for the probe centered around 580 nm in this medium. Comparison of curve a in Fig. 5 with the emission spectrum shown in Fig. 6 strongly suggests that the large emission band centered around 605 nm for the 1PAS3/C3 SAM is due to emission from the probe. The relatively weaker peaks observed at ca. 560-570 nm in both curves a and b in Fig. 5 are due to Raman scattering from bulk water in the electrochemical cell. The difference in positions for the emission maxima in Figs. 5 and 6 is not necessarily unexpected, and is likely due to subtle differences in the microscopic environment of the probe in these two cases. Ephardt and Fromherz[28] have previously discussed the solvent dependence of the emission maximum (λ_{max}) and fluorescence lifetime (τ_{obs}) of a zwitterionic derivative of this chromophore. They showed that λ_{max} ranges

from 599 to 626 nm and τ_{obs} ranges from 1.56 ns to 40 ps for CH_2Cl_2 and water, respectively, illustrating the wide range of observed values. Based on their work, it is tempting to use the λ_{max} in the SAM as an indicator of the effective polarity of the local environment. However, many other factors that influence λ_{max} may differ between bulk solution and the surface, such as ion pairing[2] and the degree of solvation of the probe[3], and such correlations are probably frought with pitfalls. Instead, we choose to view the value of λ_{max} observed in Fig. 5 as a baseline or initial condition for the chromophore in the SAM, and to then look for deviations from this value caused by purposeful variation of the applied potential.

It is important to consider the possibility that dipolar interactions between probes that were too near one another would adversely affect our interpretation of the Stark shift measurements by obscuring the interactions between the probe dipoles and the interfacial electric field. Based on expectations that such probe-probe interactions would lead to discernible variations in the λ_{max} values[42], we investigated the dependence of λ_{max} on the mole fraction of the probe in the loading solutions. The basic idea behind these experiments was to dilute the probes in the SAM sufficiently so that probe-probe dipolar interactions would be absent. In fact, when the probe mole fraction in the loading solution was decreased over a wide range (from 0.95 to 0.1), we observed a blue shift in the λ_{max} with decreasing probe mole fraction, consistent with expectations[42] that these dipolar interactions would be minimized as the probe surface coverage was reduced and, therefore, the average distance between probes was increased. The details of these experiments will be reported elsewhere. The important point is that the Stark experiments were done under conditions where it can be argued that probe-probe dipolar interactions do not influence the measurement. These were the conditions used to form the SAM's used for the Stark shift experiments and described in the *Experimental* section .

Figure 7 shows the results of *in situ* fluorescence experiments for a 1PAS3/C12 SAM on Au in 0.1 M $NaNO_3$ in which the applied potential was varied between +0.2 V and -0.5 V. Three representative spectra are shown. Note that the wavelength axis is expanded, so only the tops of the emission bands are observed. These spectra clearly show a red shift in λ_{max} as the applied potential is made more positive, and vice versa. (The vertical positions of the peaks have been arbitrarily offset for clarity. We return to a discussion of the potential dependence of the emission intensity below.) These trends in λ_{max} versus applied potential have been reproduced for many different SAM samples, and are representative of the behavior of this system. Note also that the observed, potential-dependent value of λ_{max} does not depend on the *direction* of changes in the applied potential (i.e. the shifts are not dependent on the order of the experiments).

Figure 8a shows a plot of the emission maximum for a 1PAS3/C12 sample on Au in 0.1 M $NaNO_3$ versus applied potential. In this case, the peak energy (in cm^{-1}) rather than λ_{max} is plotted, as suggested by the form of equation 1. These data show a monotonic, roughly linear relationship between the emisson peak energy and applied potential between +0.2 and -0.5 V. The line through the data points

is a linear least-squares regression fit. Similar results were obtained for several 1PAS3/C12 samples on Au substrates. Figure 8b shows plots of emission peak energy versus E_{app} for a 1PAS3/C3 on Ag in 0.1 M $NaNO_3$. The two data sets correspond to two experiments in which the direction of the change in applied potential was opposite. In the upper set, the potential was changed in the positive-going direction, and vice versa for lower set. The smaller shifts for these samples introduced more scatter in the data, but the slopes could still be reliably evaluated. The interpretation of these slopes will be presented in the *Discussion* section.

During the Stark shift measurements, it was noticed that the intensity at λ_{max} of the emission peak was reproducibly potential-dependent. Figure 9 shows this behavior for a set of scans between -0.5 and +0.5 V. For these data, replicate spectra were obtained ca. 1 minute apart at each value of applied potential, so the data appear as pairs of data points at various potentials. Two trends are evident from these data. First, there is a long term decrease in intensity. Second, the intensity is higher at positive potentials than at negative potentials. The long term decrease is likely due to a combination of photobleaching and instability of the SAM at the more positive potentials (i.e. +0.5 V). The photobleaching behavior is clearly indicated by the intensity difference for two data points in a given pair. For example, at the first application of an open circuit condition (labeled "none") the intensity decreases ca. 2% between the two replicate spectra. Similarly small, but reproducible, decreases are observed between replicate spectra for applied potentials of 0.0 and -0.5 V and at open circuit. These small changes most likely represent laser damage to the probe from irreversible photobleaching. The difference between replicate spectra is uniformly larger at an applied potential of +0.5 V, probably indicating an enhanced instability of the monolayer at positive potentials. We are uncertain of the origin of this instability, but it was routinely observed. These effects caused us to restrict the Stark measurements to potentials less than ca. +0.2 V and laser exposures as short as possible. In addition to these effects, a larger dependence of intensity on applied potential (lower intensity at less positive potentials) was also observed. This effect was quite reproducible unless the sample had been either irradiated or exposed to relatively positive potentials for too long. There are several possible explanations for this potential-dependent fluorescence intensity, including a potential dependence of the rate at which the excited state is quenched by the metal, a potential-dependent pK_a for the basic aniline functionality (i.e. more negative potentials lead to increased protonation of the probe, leading to a reduced number of emitters), an electric field-dependent transition moment, influences of ion-pairing on the fluorescence intensity, as well as others. We return to a discussion of this effect below.

Discussion

The slopes of plots of the type shown in Fig. 8 give the dependence of the Stark shift on applied potential. Equation 1 allows the potential-dependent emission peak energies to be used to calculate the

dependence of the electric field on applied potential, provided that $\Delta\mu$ and cos θ are known. As discussed above, the value of cos θ should be close to 1, so this was used in the calculation. The value of $\Delta\mu$ has been estimated both experimentally[18b] and theoretically[18a] as being about 16 Debye (5.3×10^{-29} C m). Use of these two quantities and conversion of the emission peak energy changes into units of Joules allows one to calculate the change in electric field per volt change in applied potential, which we write as $d\mathbf{E}/dE_{app}$, where $\mathbf{E}$ is the electric field and E_{app} is the applied potential. This gives values of $d\mathbf{E}/dE_{app}$ for the 1PAS3/C3 and 1PAS3/C12 cases of 4×10^4 V/cm V and 3×10^5 V/cm V, respectively. Note that these slopes refer to a change in the electric field (in V/cm) experienced by the probe *per volt change in the applied potential* (in V), as discussed above. An absolute determination of the electric field at any given potential can only be made if the potential at which the electric field is zero (i.e. the E_{pzc}) is known.

In considering the significance of these values, the size of the probe should be kept in mind. The total length of the chromophoric segment of the probe molecule is ca. 10 Å. However, the actual displacement of the electron during the emission processes (i.e. from the center of charge of the LUMO to the center of charge of the HOMO) is only ca. 3.4 Å[18]. Thus, this latter distance represents the spatial "resolution" of the measurement of electric field changes with this approach. Based on the geometric model in Scheme 1, the center of the probe is 8.5 Å from the surface. For the 1PAS3/C3 case, this center is ca. 3.5 Å from the end of the propyl chains (i.e. 3.5 Å into the diffuse layer), while for the 1PAS3/C12 case, it is approximately in the center of the alkyl chain region of the SAM.

These observed values of $d\mathbf{E}/dE_{app}$ can be compared to the results of a recent theoretical treatment by Smith and White[6], who extended the time-honored Gouy-Chapman (GC) model for the metal/electrolyte interface[5] to the case of a metal/organic monolayer/electrolyte interface. Their model is pertinent to both the 1PAS3/C3 and the 1PAS3/C12 cases, for which the probe is outside of or inside of the organic monolayer, respectively. It also allows for potential-dependent changes in the state of charge of a redox probe species within the monolayer for these two cases, a situation that is not relevant to the present case because our probe is not redox-active. Thus, when using their model, we have chosen conditions under which the charge of the hypothetical redox probe within the SAM would not depend on the applied potential (i.e. we have chosen applied potentials far from the E° of the redox probe). Then, we have used their graphical results to extract an estimate of $d\mathbf{E}/dE_{app}$ for the special case of a 1PAS3/C12 SAM. This graphical procedure is necessary because their treatment gives the interfacial potential, ϕ, as a function of distance from the metal surface, while our Stark measurements give $\mathbf{E} = -d\phi/dx$ at a particular distance from the surface. This procedure (which is only approximate), suggests that $d\mathbf{E}/dE_{app}$ for this case should be ca. 5×10^6 V/cm V, which is about an order of magnitude larger than the experimental value of 3×10^5 V/cm V. It is worth noting that, because the predicted potential drop in the interior of the SAM is linear with distance, the exact position of the probe within the SAM is not very important, so long as it is entirely contained within the alkyl chain region.

For the 1PAS3/C3 case, the comparison between model and experiment is more straightforward. Here, the Smith/White model is used to predict the total potential drop across the (dielectric) organic monolayer, then the remaining potential at the SAM/solution interface is used as an input into the limiting, exponential form of the Gouy-Chapman expression[5]. The electric field at a particular applied potential is obtained directly from the derivative of this expression evaluated 3.5 Å from the SAM/solution interface (i.e. at the center of the probe's chromophoric structure). Finally, $d\mathbf{E}/dE_{app}$ is obtained by taking the difference between two such electric field values that are calculated for two different applied potentials and normalizing to a one volt potential difference. This procedure predicts a value for $d\mathbf{E}/dE_{app}$ of 3×10^5 V/cm V. Again, the predicted value of $d\mathbf{E}/dE_{app}$ is more than an order of magnitude larger than the experimental value of 4×10^4 V/cm V. In this case, the approximately exponential decay of potential with distance makes the predicted electric field a strong function of the exact position of the probe within the decay region. This, coupled with the relatively large size of the chromophoric segment of the probe, increases the uncertainty of the predicted electric field for this case.

These comparisons of the predicted and observed values of $d\mathbf{E}/dE_{app}$ reveal large discrepancies between theory and experiment for these cases. There are at least three possible sources for this. One is the presence of phenomena that individually or collectively conspire to decrease the observed spectral shifts, and another is the presence of phenomena that significantly influence the interfacial potential profile but are not embodied in the theoretical models. An example of the first type would be a solvatochromic effect[43] due to potential-dependent changes in the interfacial dielectric constant. However, this seems fairly unlikely since virtually all theoretical models of the double layer that include dipolar solvent structures indicate that dielectric saturation is rarely, if ever, encountered.[44] Another possible source of experimental problems would be a shift in the emission spectrum caused by essentially the same effects that lead to energy transfer to the metal, namely, coupling between the probe electronic structure and that of the metal.[45a] However, these shifts have been estimated[45b] to be in the range of 1 - 10 cm^{-1} at the plasmon frequency for the metal, and much lower (< 1 cm^{-1}) at frequencies away from the plasmon frequency as is the case here, suggesting that this effect cannot be responsible for the much larger shifts observed here.

Another possible source of Stark shifts that are smaller than expected is a change in the net orientation of the probe species within the monolayer in response to variations in E_{app}, where these changes are in the direction of decreasing interaction between $\Delta\mu$ and ΔE. A discussion this effect depends on a knowledge of the E_{pzc}. While the value of E_{pzc} is not directly available for these SAM's, it is possible to make reasonable assumptions that allow one to estimate it. Bryant and Crooks[46] have demonstrated the use of differential capacitance to determine the E_{pzc} for an alkyl thiol SAM on Au, and obtained a value of +0.2 V, which is consistent with previous determinations for the E_{pzc} at bare Au under a variety of conditions.[46] This indicates that the presence of the SAM does not significantly change the

E_{pzc}. Given this situation for Au, it seems reasonable to make the same assumption about alkyl thiol SAM's on Ag, for which the E_{pzc} is reported as -0.79 V.[47] Thus, for the experiments described above for the 1PAS3/C3 SAM's on Ag substrates, the applied potential was always positive of E_{pzc}, while for the 1PAS3/C12 case on Au, the applied potential was always negative of E_{pzc}. Under these conditions, the ground state dipole moment of the probe (which has a value of 10 D) is unfavorably oriented with respect to the electric field for the 1PAS3/C3 case, while it is favorably oriented for the 1PAS3/C12 case. For the probe excited state, the dipole moment is reversed in direction but also is smaller (about -6 D), which will mitigate against strong effects of the electric field on its orientation.

The ability of the interfacial electric field to influence the probe's orientation depends on the energy of interaction between the dipole moment of the probe and the interfacial electric field. For the ground state, this energy is 4×10^{-22} J for a field strength of 10^5 V/cm. Comparison of this energy with the available thermal energy at room temperature ($1.5\ kT = 6 \times 10^{-21}$ J) indicates that the electrostatic interaction is a significant fraction of the available thermal energy, implying that probe reorientation is possible under these circumstances. Thus, the unfavorable orientation of the probe ground state dipole moment with respect to the electric field for the 1PAS3/C3 SAM's on Ag may have led to an (unmeasured, and therefore, unknown) increase in θ toward 90° , and a correspondingly smaller Stark shift and calculated electric field. This possibility seems especially likely for this case because orientation of the probe along the surface normal is not reinforced within the SAM by strong interactions with long alkyl chains as it is for the 1PAS3/C12 case. These considerations lead to the conclusion that the electric field strengths observed for the 1PAS3/C3 SAM's are likely to be too small, and that the discrepancy between the predicted and observed dE/E_{app} values is due to ground state probe reorientation under the influence of the interfacial field. On the other hand, for the 1PAS3/C12 SAM's on Au, the combination of a favorable orientation of the ground state dipole moment and the orienting influence of the alkyl chains of the dodecanethiol probably prevents significant changes in the ground state orientation of the probe.

A related possibility that was mentioned above is that the orientation of the excited state species may change due to unfavorable interaction between its dipole moment and the electric field. Note that this could only happen for the 1PAS3/C12 SAM's on Au, where the excited state orientation is unfavorable at the applied potentials used for the measurements. Again, the ordering influence of the dodecanethiol matrix should work against such reorientation. Further, for such an effect to influence the Stark measurements, it would have to occur on a timescale comparable to or shorter than the fluorescence lifetime, τ_{obs}. Since τ_{obs} is likely to be in the 10-100 ps range[28,45a], this reorientation in the excited state would need to be *very* fast. At the present time, we have no way of evaluating the rate at which such motions could occur in such a monolayer system, so this possibility can be neither rejected nor substantiated. However, the combination of a smaller electrostatic interaction energy between the excited

state dipole moment and the field, the ordering influence of the SAM, and the lifetime argument just presented make it seem unlikely that probe reorintation would be significant for the 1PAS3/C12 case. Taken in total, these considerations of all of the possible "experimental" difficulties with the Stark measurements suggest that the measurement of interfacial electric fields that are smaller than predicted by the models is likely a real effect, at least for the 1PAS3/C12 case.

Turning now to the theoretical models, it seems that there are two phenomena that could be at work in producing overly large predicted values for the interfacial electric fields. First, the Smith/White model neglects discreteness-of-charge effects, which will act to reduce the predicted field. Fawcett has shown how these can be simply introduced, and has estimated the magnitude of such effects on the predicted electric fields.[48] Generally, inclusion of these effects will reduce the predicted fields by a factor of 2-3, a significant change, but not sufficient to bring the experimentally and theoretically predicted fields into substantial agreement. A second phenomenon that has not been considered theoretically before in this context is related to the presence of charge-compensating counterions within the SAM. In all of our previous studies of SAM's containing charged groups, the EQCM results have clearly indicated the presence of mobile counterions within the SAM[2,3]. Thus, it is to be expected that the cationic charge of the probe species in the 1PAS3/C12 monolayer would cause an anion from the supporting electrolyte to remain fixed within the SAM, probably relatively near to the pyridinium cationic center. In such a case, one could argue that when large electric fields are applied across the monolayer, these mobile counterions would be displaced by an amount and direction that would depend on the magnitude and orientation of the electric field. Then, this small displacement of the mobile counterion would serve the function of providing a type of electrostatic screening for the probe species. In essence, the local potential drop due to the charge separation of the fixed cationic site on the probe and the mobile anion, which might occur over distances of only a few Å, would reduce the potential drop aross the chromophoric region of the probe, thereby reducing the observed Stark shift. Based on all of the considerations described above for the 1PAS3/C12 case, we would argue that the experimental value of dE/dE_{app} is probably a real measure of the effective interfacial electric field experienced by the probe, and that the discrepancy between the predicted and observed electric field strengths results from a combination of neglect of such electrostatic screening effects and discreteness-of-charge effects.

The dependence of emission intensity on E_{app} shown in Figure 9 is worth revisiting. As mentioned above, this effect could be due to several phenomena. It is interesting to consider the last one that was presented, namely, an electric field-dependent transition moment. The influence of an electric field on the transition for an electronic transition has been discussed by Liptay[43], and is given by:

$$\mu_{ge}^{E} = \mu_{ge} + \Delta\alpha_{ge} E \qquad (4)$$

where μ_{ge}^{E} is the transition moment for the electronic transition in the presence of the field, μ_{ge} is the transition moment in the absence of the field, $\Delta\alpha_{ge}$ is the change in the polarizability tensor between the

ground state and the excited state, and E is the the electric field. Note that this equation is written for the special case in which the directions of the transition moment, the polarizability change, and the electric field are all the same, along the long axis of the probe. This is reasonable for the present case, since μ_{ge} and $\Delta\alpha_{ge}$ are known to be along the long axis of chromophores of this type[49] and the long axis is thought to be along the surface normal, and therefore, parallel to **E**. Typically, the influence of the $\Delta\alpha_{ge}$ E term is not observed, both because $\Delta\alpha_{ge}$ is not usually very large and because large values of E are not easily attainable in more traditional Stark experiments.[49] However, in the present case $\Delta\alpha_{ge}$ is probably not insignificant, based on the value of 1.67×10^{-38} C m^2/V reported[49] for the compound 4-dimethylamino-4'-nitrostilbene, which has a donor-acceptor electronic structure and a large dipole moment change between ground and excited states that is very similar to that of the (dimethylaminostyryl)pyridinium probe used here[50]. Using this value, a rough estimate of the $\Delta\alpha_{ge}$ E term for the present case is 0.15 D (or 5×10^{-31} Cm) for a field strength of 3×10^5 V/cm. This is only about 1% of the value of the transition moment calculated from the oscillator strength using the absorption spectrum (from which a value of 12 D was obtained). Since the molar absorptivity (and therefore the excitation rate in the Stark shift experiments) is proportional to the square of the transition moment, these calculations suggest that intensity variations due to an electric field-dependent transition moment should be on the order of 1-2%. In fact, the observed variations are closer to 10% of the total emission intensity (corrected for background). These considerations suggest that the major fraction of the potential-dependence of the fluorescence intensity derives from some other process, such as a potential-dependent quenching rate, protonation behavior at the nitrogen of the dimethylamino group, or fluorescence quantum yield (vide infra). However, should conditions be achieved in which the applied electric fields reach values of 10^6 - 10^7 V/cm, the potential dependence of the transition moment would likely lead to a very significant dependence of emission intensity on applied potential. Of course, such conditions would also lead to much larger Stark shifts, and to an increase of the relative importance of the quadratic term in equation 1.

We now briefly discuss a previous study of the (dimethylaminostyryl)pyridinium chromophore and its relevance to the present work. Ephardt and Fromherz[28] have made a very detailed investigation of the dynamics of the fluorescence process for this compound. They measured the dynamics and the ratio of quantum yields of the trans-to-cis and cis-to-trans photoisomerizations (ϕ_{TC}/ϕ_{CT}), and found that this ratio depends on the medium, varying between 0.006 (for water) and 0.087 (for lecithin membranes). They also determined that the rate constants for the interconversions between the various states that connect the cis and trans forms are on the order of 0.1 - 10 ns^{-1}. These results indicate that the photostationary state (i.e. constant trans and cis concentrations under irradiation) would be reached under our conditions essentially immediately, and that this state will be comprised predominantly of the trans isomer. Thus, the long term changes in fluorescence intensity that we observed (see Fig. 9) cannot be due to interconversions between the trans and cis forms of the probe. They also showed that the excited state of

this probe has a non-radiative deactivation pathway that involves formation of a twisted internal charge transfer (TICT) state that rapidly internally converts to the ground state. They speculated that this TICT state may involve rotation around the aniline-ethylene bond. The rate of formation of the TICT state from the fluorescent state (F) was shown to be strongly dependent on the viscosity of the solvent, with the friction caused by more viscous solvents leading to a reduced rate, and therefore, a higher fluorescence quantum yield (ϕ_F). For example, ϕ_F values in methanol and dodecanol are 0.013 and 0.41, respectively.[28] These results imply that ϕ_F might depend on the type of SAM used for our experiments, with the 1PAS3/C3 monolayers expected to exhibit considerably smaller values than those for the 1PAS3/C12 monolayers. Unfortunately, it is nearly impossible to make absolute comparisons of fluorescence intensity between different samples with our experimental system because of the difficulty in reproducible sample placement, so we have not been able to investigate this effect. Nevertheless, these considerations do suggest that higher intensities should be obtained with the 1PAS3/C12 monolayers, which is useful information in terms of experimental design for such studies.

Finally, we discuss the use of molecules such as the (dimethylaminostyryl)pyridinium probe in non-linear optical applications such as second harmonic generation (SHG), because of its direct relevance to our results. Marks and coworkers[50-52] have published several reports of the fabrication of monolayer and multilayer assemblies of this molecule (or derivatives of it) and of the SHG efficiency of these assemblies. Just as is the case for the Stark effect measurements here, their SHG experiments rely on an ability to produce net orientation of the probe at a surface. It is particularly significant that they have observed a strong influence of the SHG efficiency for these assemblies on the nature of the anionic counterion within the assembly, with increases as large as 44% associated with the change from a Cl^- to an ethyl orange counterion.[52] Computational results suggest that this effect arises from a change in the polarizability of the probe due to the nature and position of the anion with respect to the cationic charge of the (dimethylaminostyryl)pyridinium moieties.[50] Stated more generally, the nature and extent of electrostatic interactions (such as ion-pairing) between the probe and its counterion within the assembly can be expected to significantly influence the electronic structure of the probe. Given that the SHG efficiency (measured by β, the hyperpolarizability) is proportional to μ_{ge}^2 and $\Delta\mu$[53], we would expect that these interactions would also manifest themselves in variations in both the fluorescence intensity and the value of λ_{max} for our experiments. This suggests that the discrepancies between the predicted and observed dE/dE_{app} values for the 1PAS3/C12 case, as well as the observed dependence of the fluorescence intensity on applied potential, may be related to the influence of the interfacial electric field on the position of the counterion, and therefore, on the electrostatic interactions between it and the probe. These arguments can be used to qualitatively explain the results in Fig. 9. For example, at more positive potentials, the anionic counterions would be displaced away from the probe, toward the positively charged electrode surface. This would decrease the interaction between the anion and the cationic site on the

probe. Since this interaction decreases μ_{ge} (because the presence of the anion opposes the charge shift from the donor site to the acceptor site that occurs during the CT transition), displacement of the anion should lead to an increase in fluorescence intensity, as is observed.

Conclusions

The results presented above represent the first application of fluorescence Stark effect measurements to the determination of electric fields at electrode-electrolyte interfaces. Two cases were examined, 1PAS3/C3 monolayers on Ag and 1PAS3/C12 monolayers on Au, for which the probe species is outside of or inside of the SAM structure, respectively. For both cases, the experimentally observed interfacial electric fields are significantly less than those predicted by existing models. However, we believe the reasons for these discrepancies are different for the two cases. For the former case, the influence of the electric field is likely to produce a probe orientation that is more parallel than perpendicular to the surface, leading to an underestimation of the electric field. For the latter case, several factors probably enter into play, including discreteness-of-charge effects, electrostatic screening from electric field-induced counterion displacement within the SAM, and influence of the counterion within the SAM on the polarizability of the probe, and therefore on $\Delta\mu$ and μ_{ge}. This interpretation suggests that two separate types of effects need to be better addressed in the models that are used to describe such phenomena. First, more realistic models of interfacial potential profiles will likely need to take into account the presence of ions and the possibility of electric field-induced displacements of these within interfacial assemblies. Second, whenever probes are used to investigate the interfacial environment, one must always consider the consequences of local effects due to the presence of the probe, because these may alter its behavior thereby inhibiting its ability to accurately report on its environment. In the present case, these effects manifest as an influence of the probe's counterion both on its ability to accurately sense the interfacial field and on the spectral properties of the probe that are used to determine the interfacial field.

One way of obviating these influences of counterions within the SAM is to use a neutral probe species. A promising candidate for this extension of the present study is a derivative of 4-dialkylamino-4'-nitrostilbene that is suitably functionalized to allow it to be immobilized within these alkyl thiol-based SAM's. This compound has very similar spectral properties to those of the (dimethylamino)pyridinium probe used here.[43,50,53] Efforts to employ this approach are currently underway.

Another important conclusion of the present work is that fluorescence measurements on species present at metal surfaces are both possible and understandable based on the simple notions embodied in equation 3. These considerations suggest that fluorescence measurements such as those reported here will be possible any time the radiative rate is competitive with the non-radiative processes that lead to deactivation of the excited state. Thus, a simple criterion for predicting the probability of success in such

measurements will be the shortness of the intrinsic fluorescence lifetime of the emitter, with shorter lifetimes being expected to produce higher fluorescence intensities.

As is clear from the discussion above, there are many, diverse physical phenomena that collectively operate to produce the observed potential-dependent fluorescence intensities and λ_{max} values. Distinguishing between them will require considerable care in experimental design and execution. Nevertheless, such an endeavor would seem to be very worthwhile because the results of such experiments speak directly to the influence of the interfacial environment on the behavior of molecules that find themselves there, a goal that ultimately must be achieved to fully understand electrochemical phenomena.

Acknowledgments

We are grateful to the Office of Naval Research for full support of this work.

References

1. Ulman, A. *An Introduction to Ultrathin Organic Films from Langmuir-Blodgett to Self-Assembly*; Academic Press: New York, 1991.
2. a) De Long, H. C., Buttry, D. A. *Langmuir*, **1990**, *6*, 1319-22. b) De Long, H. C.; Donohue, J. J.; Buttry, D. A. *Langmuir*, **1991**, *7*, 2196-2202.
3. De Long, H. C., Buttry, D. A. *Langmuir*, **1992**, *8*, 2491-96.
4. Grahame, D. C. *Chem. Rev.*, **1947**, *41*, 441.
5. Bard, A. J.; Faulkner, L. R. *Electrochemical Methods*; J. Wiley: New York, 1980.
6. Smith, C. P.; White, H. S. *Anal. Chem.*, **1992**, *64*, 2398-2405.
7. a.) Marra, J.; Israelachvili, J. N. *Biochemistry*, **1985**, *24*, 4608-18. b.) Marra, J. *J. Phys. Chem.*, **1986**, *90*, 2145-50.
8. Pashley, R. M.; McGuiggan, P. M.; Ninham, B. W.; Brady, J.; Evans, D. F. *J. Phys. Chem.*, **1986**, *90*, 1637-42.
9. Evans, E. A.; Parsegian, V. A. *Proc. Natl. Acad. Sci. U.S.A.*, **1986**, *83*, 7132-36.
10. Winiski, A. P.; Eisenberg, M.; Langer, M.; McLaughlin, S. *Biochemistry*, **1988**, *27*, 386-92.
11. Pope, J. M.; Tan, Z.; Kimbrell, S.; Buttry, D. A. *J. Am. Chem. Soc.* **1992**, *114*, 10085-6.
12. Waggoner, A. S. *J. Membr. Biol.*, **1976**, *27*, 317-30.
13. Reich, R.; Scheerer, R. *Ber. Bunsenges. Phys. Chem.*, **1976**, *80*, 542-547.
14. a) Plieth, W. J.; Gruschinske, P.; Hensel, H.-J. *Ber. Bunsenges. Phys. Chem.*, **1978**, *82*, 615-20. b) Schmidt, P. H.; Plieth, W. J. *J. Electroanal. Chem.*, **1986**, *201*, 163-74. c) Korzeniewski, C.; Shirts, R. B.; Pons, S. *J. Phys. Chem.*, **1985**, *89*, 2297-8. d) Russell, A. E.; Pons, S.; Anderson, M. R. *Chemical Physics*, **1990**, *141*, 41-49.
15. Liptay, W. *Angew. Chem. Int. Ed. Engl.*, **1969**, *8*, 177-88.
16. Platt, J. R. *J. Chem. Phys.*, **1961**, *34*, 862-67.
17. Platt, J. R. *J. Chem. Phys.*, **1955**, *23*, 1833-37.
18. a.) Loew, L. M.; Bonneville, G. W.; Surow, J. *Biochemistry*, **1978**, *17*, 4065-71. b.) Loew, L. M.; Simpson, L. L. *Biophys. J.*, **1981**, *34*, 353-65.
19. Kuhn, H. *J. Chem. Phys.*, **1970**, *53*, 101-112.
20. Chance, R. R.; Prock, A.; Silbey, R. in *Advances in Chemical Physics*; Rice, S. A.; Prigogine, I.; Eds.; Wiley: New York, 1978; Vol. 37, p. 1.
21. Chen, S. H.; Frank, C. W. *Langmuir*, **1991**, *7*, 1719-26.
22. Weitz, D. A.; Garoff, S.; Gersten, J. I.; Nitzan, A. *J. Chem. Phys.*, **1983**, *78*, 5324-38.
23. Weitz, D. A.; Garoff, S.; Hanson, C. D.; Gramila, T. J.; Gersten, J. I. *Optics Lett.*, **1982**, *7*, 89-91.
24. Wokaun, A.; Lutz, H.-P.; King, A. P.; Wild, U. P.; Ernst, R. R. *J. Chem. Phys.*, **1983**, *79*, 509-14.
25. Naujok, R. R.; Duevel, R. V.; Corn, R. M. *Langmuir*, **1993**, *9*, 1771-4.

26. Hashimoto, K.; Hiramoto, M.; Sakata, T.; Muraki, H.; Takemura, H.; Fujihira, M. *J. Phys. Chem.*, **1987**, *91*, 6198-6203.
27. Zhao, X.; Christ, C. S.; Van Ryswyk, H.; Silbey, R. J.; Wrighton, M. S. *J. Phys. Chem., in press.*
28. Ephardt, H.; Fromherz, P. *J. Phys. Chem.*, **1989**, *93*, 7717-25.
29. Hassner, A.; Birnbaum, D.; Loew, L. M. *J. Org. Chem.*, **1984**, *49*, 2546-51.
30. Bain, C. D.; Troughton, E. B.; Tao, Y.-T.; Evall, J.; Whitesides, G. M.; Nuzzo, R. G. *J. Am. Chem. Soc.*, **1989**, *111*, 321-35.
31. Arisawa, S.; Yamamoto, R. *Langmuir*, **1993**, *9*, 1028-30.
32. a) Van Huong, C. N.; Parsons, R.; Marcus, P.; Montes, S.; Oudar, J. *J. Electroanal. Chem.*, **1981**, *119*, 137-48. b) Hamelin, A.; Stoicoviciu, L. *J. Electroanal. Chem.*, **1987**, *234*, 93-105.
33. Su, W.-F. A.; Kurata, T.; Nobutoki, H.; Koezuka, H. *Langmuir*, **1992**, *8*, 915-19.
34. Allara, D. L.; Nuzzo, R. G. *Langmuir* **1985**, *1*, 52-66.
35. Debe, M. K. *Appl. Surf. Sci.*, **1982-82**, *14*,1-40.
36. Greenler, R. G. *J. Chem. Phys.*, **1966**, *44*, 310-315.
37. Pemberton, J. E.; Bryant, M. A.; Sobolinski, R. L.; Joa, S. L. *J. Phys. Chem.*, **1992**, *96*, 3776-82.
38. Ziolo, R. F.; Gunther, W. H. H.; Meredith, G. R.; Williams, D. J.; Troup, J. M. *Acta Cryst.*, **1982**, *B38*, 341-43.
39. a) Laibinis, P. E.; Whitesides, G. M.; Allara, D. L.; Tao, Y.-T.; Parikh, A. N.; Nuzzo, R. G. *J. Am. Chem. Soc.*, **1991**, *113*, 7152-67, b) Walczak, M. M.; Chung, C.; Stole, S. M.; Widrig, C. A.; Porter, M. D. *J. Am. Chem. Soc.* **1991**, *113*, 2370-78.
40. Nordyke, L. L.; Buttry, D. A. *Langmuir*, **1991**, *7*, 380-388.
41. Shibasaki, K.; Itoh, K. *J. Raman Spectr.*, **1991**, *22*, 753-58.
42. a.) Evans, C. E.; Song, Q.; Bohn, P. W. *J. Colloid Int. Sci.*, **1994**, *166*, 95-101; b.) Czikklely, V.; Forsterling, H. D.; Kuhn, H. *Chem. Phys. Lett.*, **1970**, *6*, 207-10.
43. Liptay, W. *Angew. Chem. Internat. Ed.*, **1969**, *8*, 177-188.
44. Kenkel, S. W.; Macdonald, J. R. *J. Chem. Phys.*, **1984**, *81*, 3215-20.
45. a) Chance, R. R.; Prock, A.; Silbey, R. *J. Chem. Phys.*, **1976**, *65*, 2527-31. b.) Chance, R. R.; Prock, A.; Silbey, R. *Phys. Rev. A*, **1975**, *12*, 1448-52.
46. Bryant, M. A.; Crooks, R. M. *Langmuir*, **1993**, *9*, 385-7.
47. a) Valette, G.; Hamelin, A. *J. Electroanal. Chem.*, **1973**, *45*, 301-304. b) Valette, G.; Hamelin, A. *J. Electroanal. Chem.*, **1982**, *131*, 299-308.
48. a) Fawcett, W. R. *J. Electroanal. Chem.*, **1994**, *378*, 117-24, b) Fawcett, W. R.; Fedurco, M.; Kovacova, Z. *Langmuir*, **1994**, *10*, 2403-2408.
49. Liptay, W. *In "Excited States"*; Lim, E. C., Ed.; Academic Press: New York, 1974; Vol. 1; pp. 129-229.
50. Marks, T. J.; DiBella, S.; Fragala, I. *Chem. Mater.*, **1995**, *7*, 400-405.
51. Yitzchaik, S.; Roscoe, S. B.; Kakkar, A. K.; Allan, D. S.; Marks, T. J.; Xu, Z.; Zhang, T.; Lin, W.; Wong, G. K. *J. Phys. Chem.*, **1993**, *97*, 6958-60.
52. Roscoe, S. B.; Yitzchaik, S.; Kakkar, A. K.; Marks, T. J.; Lin, W.; Wong, G. K. *Langmuir*, **1994**, *10*, 1337-39.
53. Kanis, D. R.; Ratner, M. A.; Marks, T. J. *Chem. Rev.*, **1994**, *94*, 195-242.

Figure Captions

1. Structural representations of: a) hemicyanine (*trans*-4[4-(Dimethylamino)styryl] pyridine); b) 1PAS3Br; and c) 1PAS3SH.

2. Reflection absorption FTIR spectrum of a 1PAS3/C12 monolayer on smooth gold loaded for 21 hours from a solution of 0.9:0.1 molar fraction of 1PAS3SH:C12SH. Spectrum represents 2048 co-added scans at 2 cm^{-1} resolution. Line is equal to 0.001 absorbance units.

3. Transmission FTIR spectrum of bulk 1PAS3SH. Spectrum represents 256 co-added scans at 2 cm^{-1} resolution.

4. Surface enhanced Raman spectrum of a 1PAS3/C2 monolayer on roughened silver relative to the 5145 Å laser line. The laser power was ca. 50 mW and controlled via feedback. Entrance slit was 2 mm wide. Throughout the scan, the monolayer substrate was biased to -0.8 V vs. an Ag/AgCl reference electrode in 0.1 M Na_2SO_4.

5. *In situ* fluorescence spectra of a bare roughened gold substrate (b) and of the same substrate supporting a 1PAS3/C3 monolayer in 0.1 M $NaNO_3$ (a). Laser power was ca. 3 mW controlled via feedback of the 476.5 nm line. Spectra represent 5 co-added exposures of 10 seconds each.

6. Bulk excitation/emission spectra of 1PAS6SH in 0.1 M Na_2SO_4.

7. Representative Stark spectroscopy data of the fluorescence emission peak of a 1PAS3/C12 monolayer at three potentials in 0.1 M $NaNO_3$. Laser power was ca. 3 mW controlled via feedback of the 476.5 nm line. Spectra represent 5 co-added exposures of 5 seconds each.

8. a.) Plot of emission peak energy in wavenumbers versus applied potential for the data shown in Figure 7. The line represents the least-squares regression (slope is -86.9, $r^2 = 0.9$) for the data set. b.) Plot of emission peak energy in wavenumbers versus applied potential for a 1PAS3/C3 monolayer. For the upper set of data the potential was changed in a positive-going direction, and the line represents the least-squares regression to that data set (slope is -10.7, $r^2 = 1.0$). For the lower set of data the potential was changed in a negative-going direction, and the line represents the least-squares regression to that data set (slope is -15.1, $r^2 = 0.7$).

9. Plot of relative maximum intensity of the emission peak of a 1PAS3/C6 monolayer vs. applied potential. Spectra were taken in sets of two at the same applied potential before the potential was changed. The laser beam was not blocked from the surface between spectra in the sets (e.g. between the first and second spectra) but was blocked between sets (e.g. between the second and third spectra). "None" refers open circuit conditions. Spectra represent 5 co-added scans of 5 seconds each. Laser power was ca. 3 mW controlled via feedback of the 476.5 nm line.

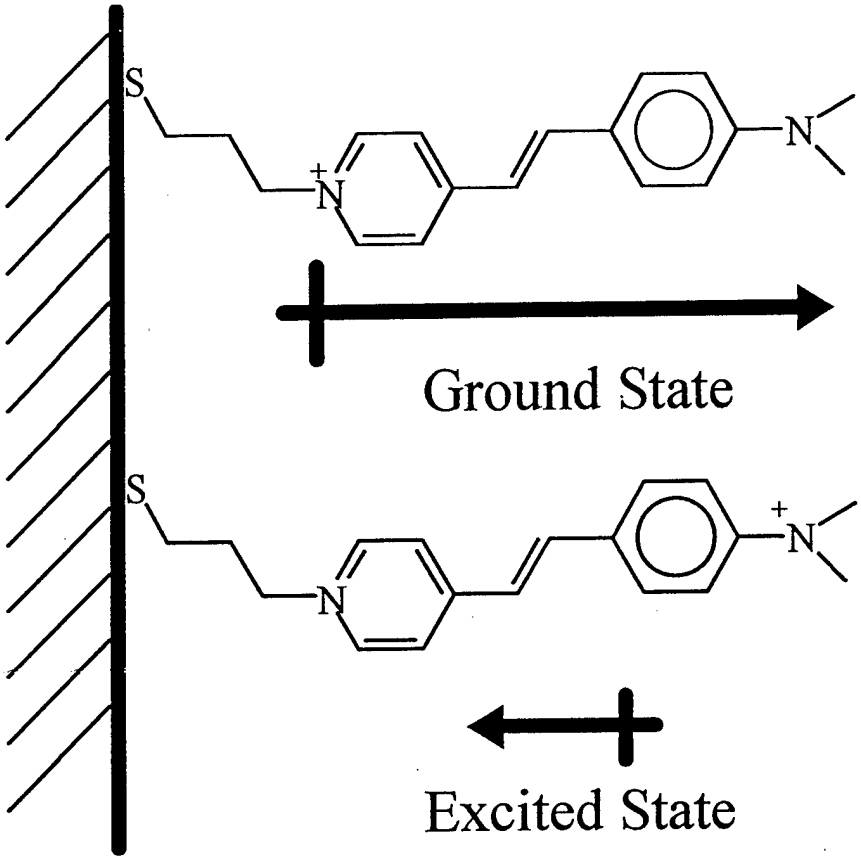
S
+
N
N
Ground State
S
N
+
N
Excited State

a. 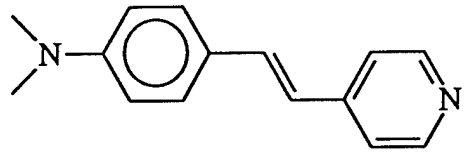

b. 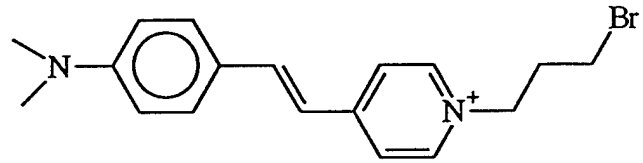

c. 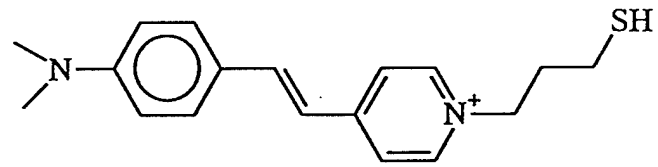

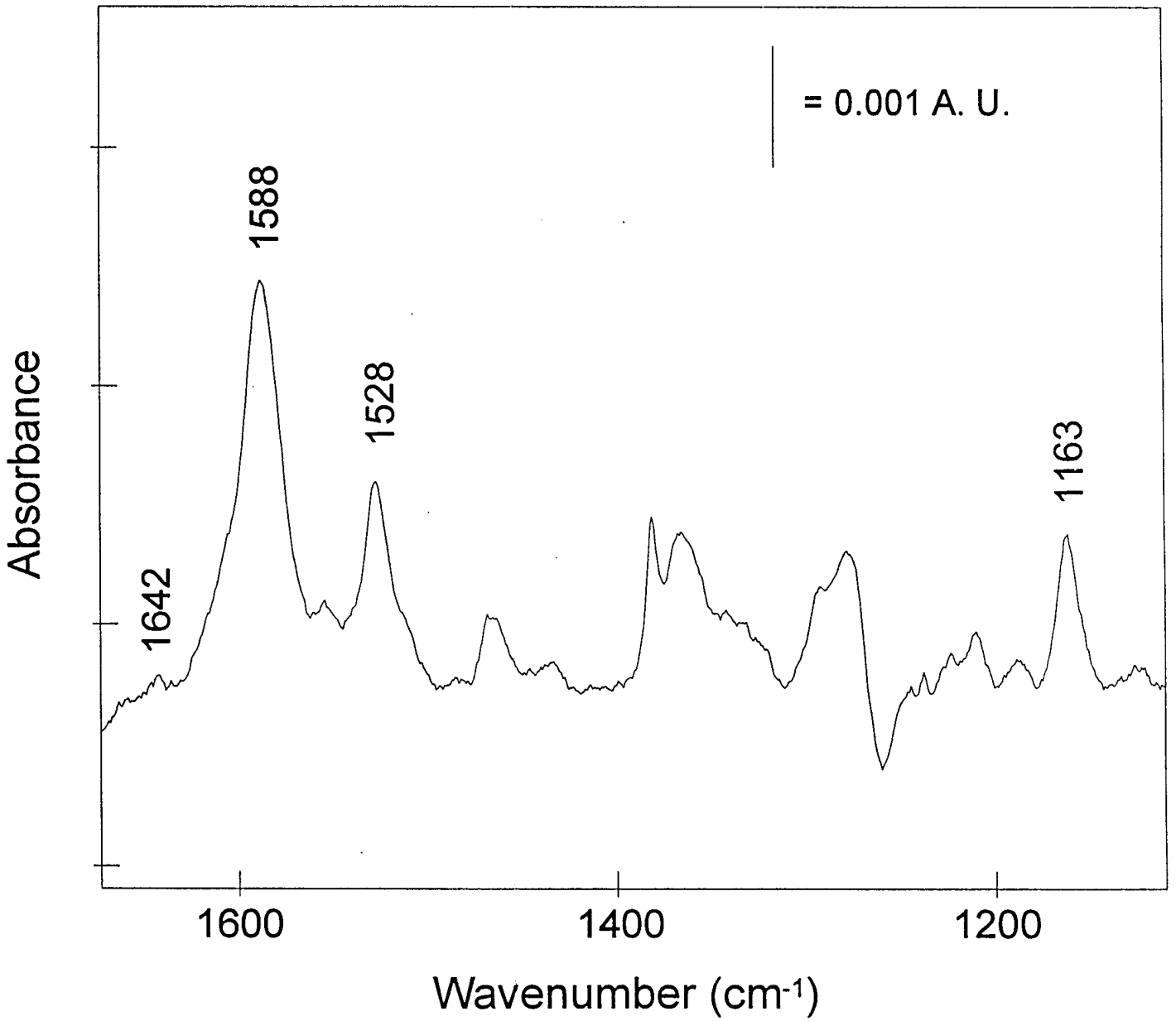
= 0.001 A. U.
1588
1528
1642
1163
Absorbance
1600
1400
1200
Wavenumber (cm-1)

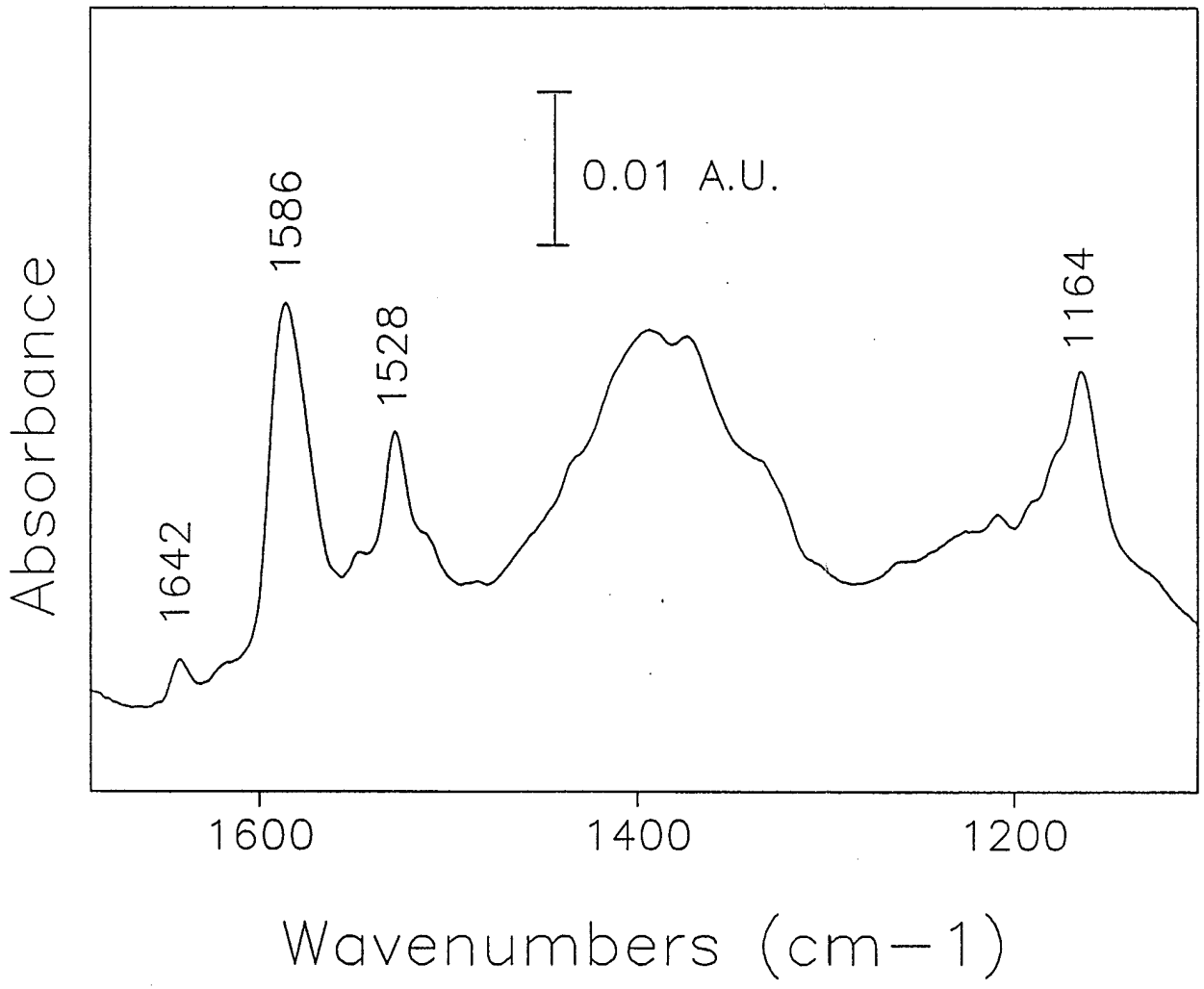
Absorbance
1642
1586
1528
0.01 A.U.
1164
1600
1400
1200
Wavenumbers (cm−1)

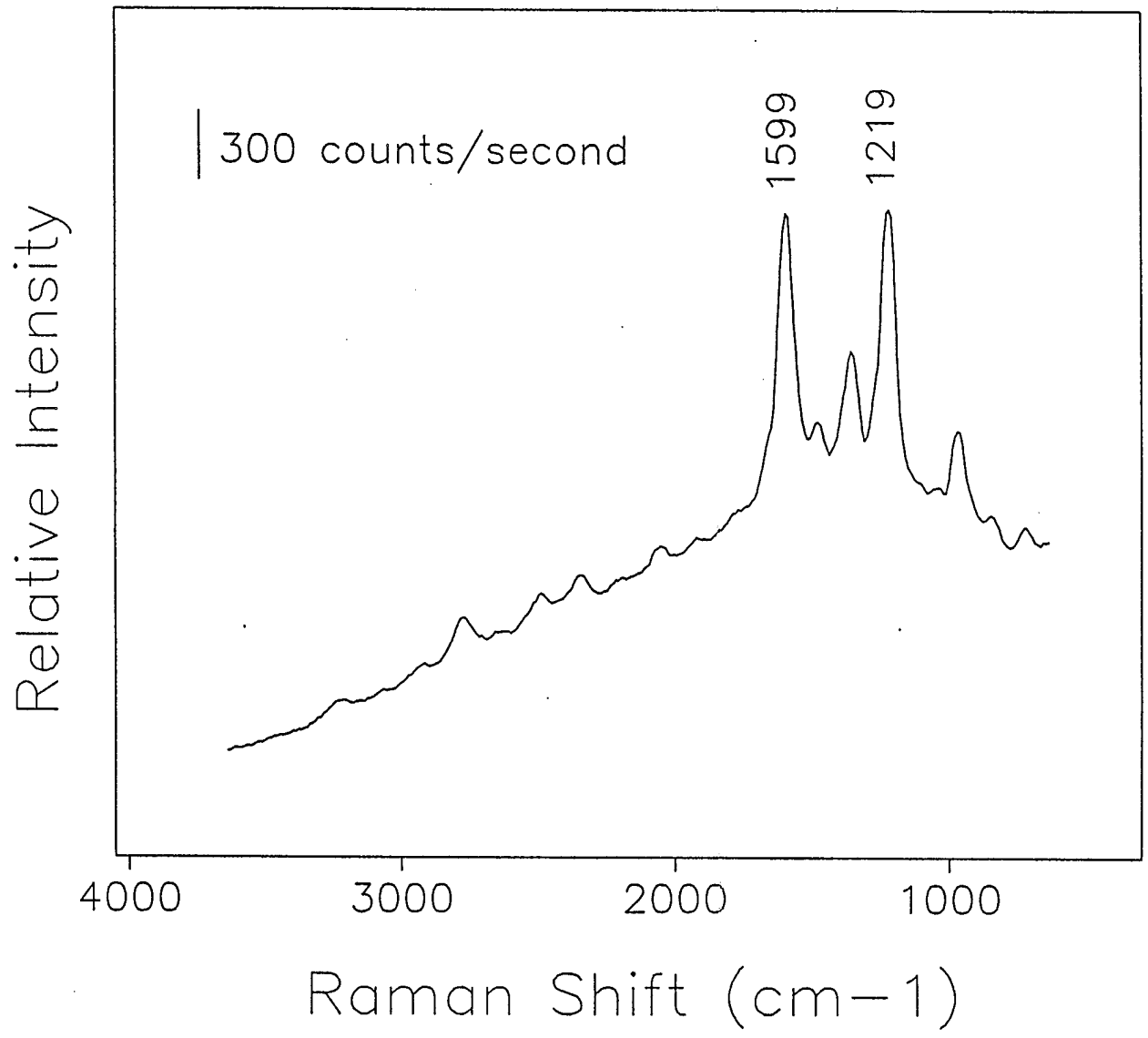
300 counts/second
1599
1219
Relative Intensity
4000
3000
2000
1000
Raman Shift (cm−1)

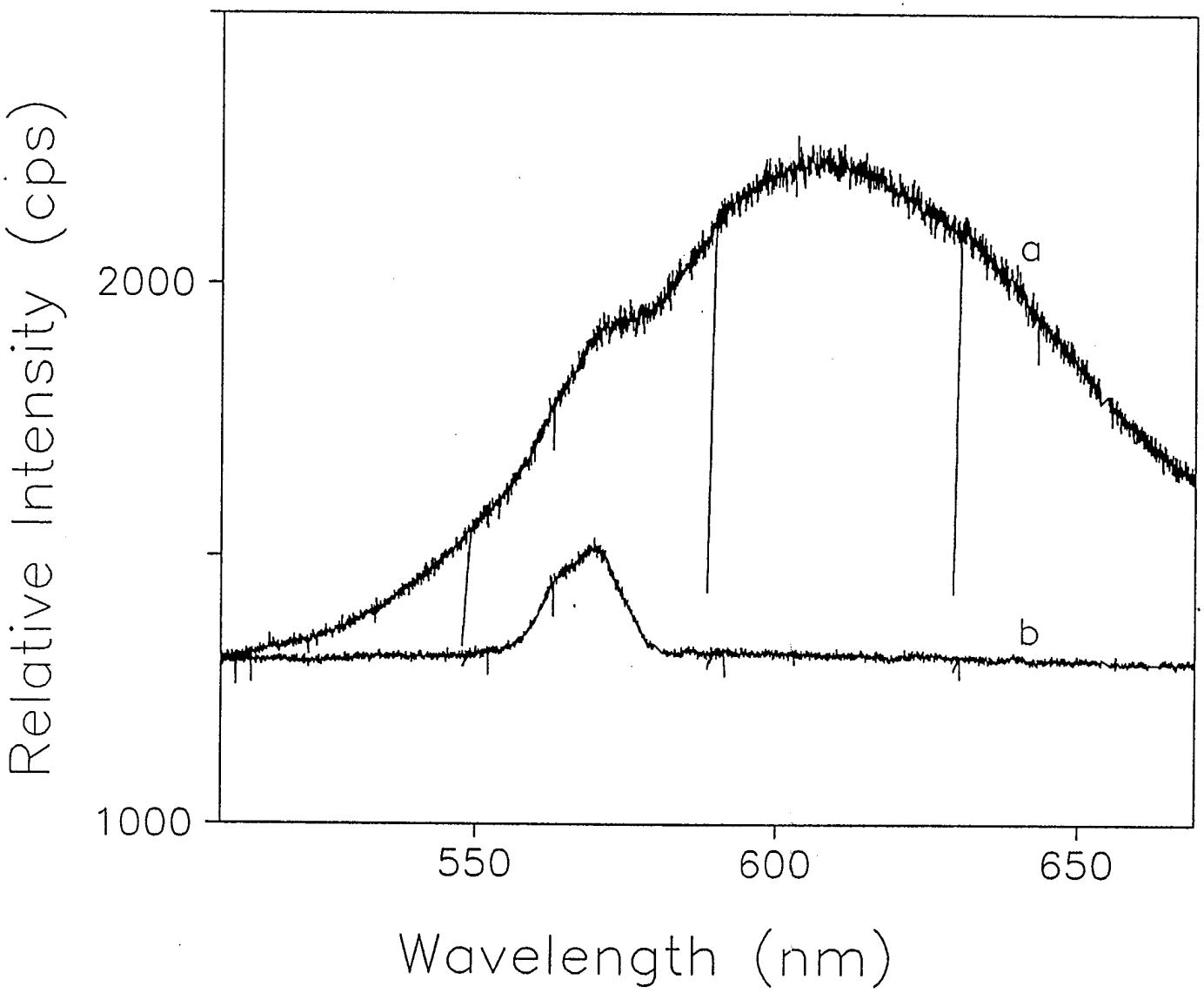
Relative Intensity (cps)
2000
1000
550
600
650
Wavelength (nm)
a
b

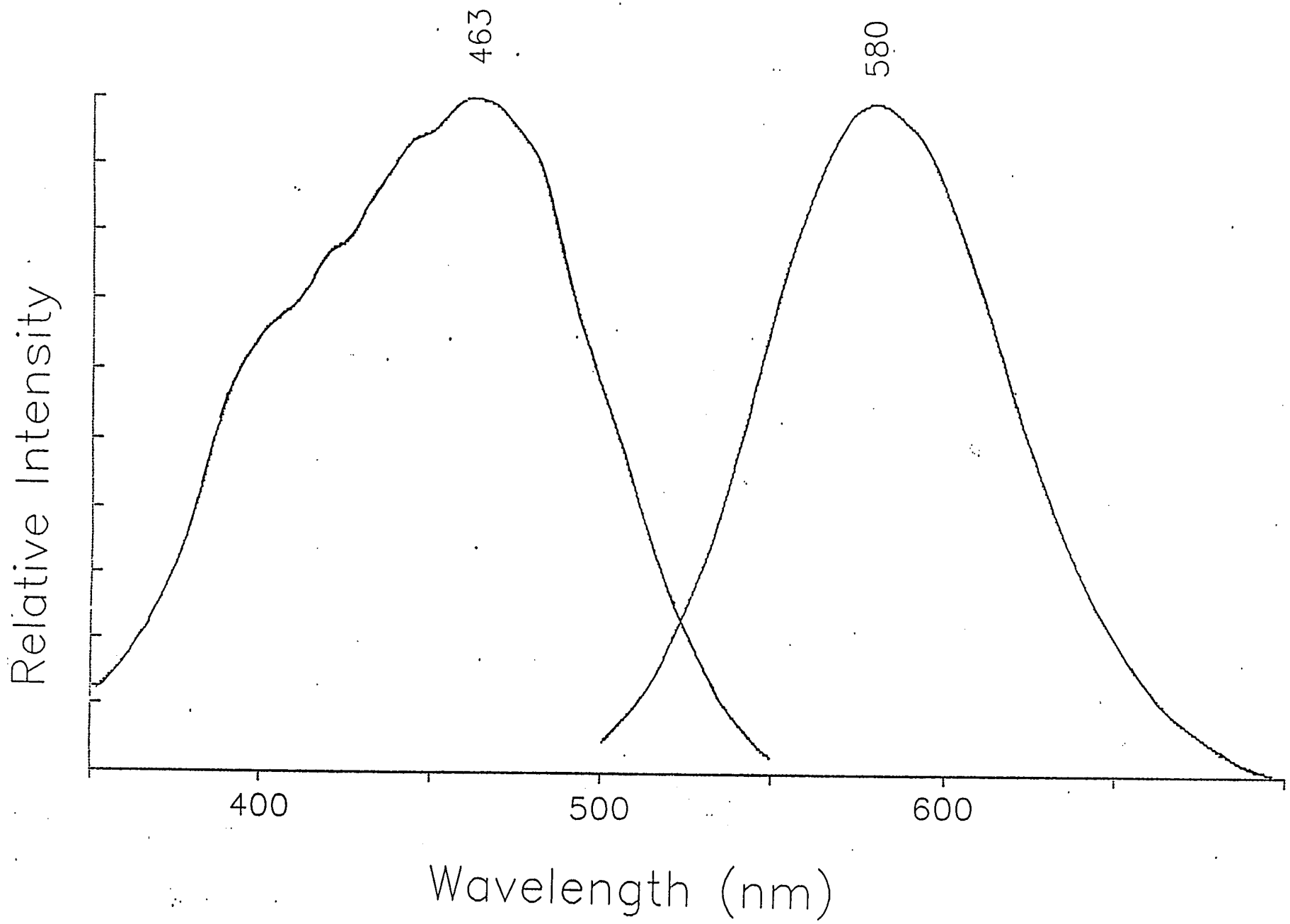

Fig. 5

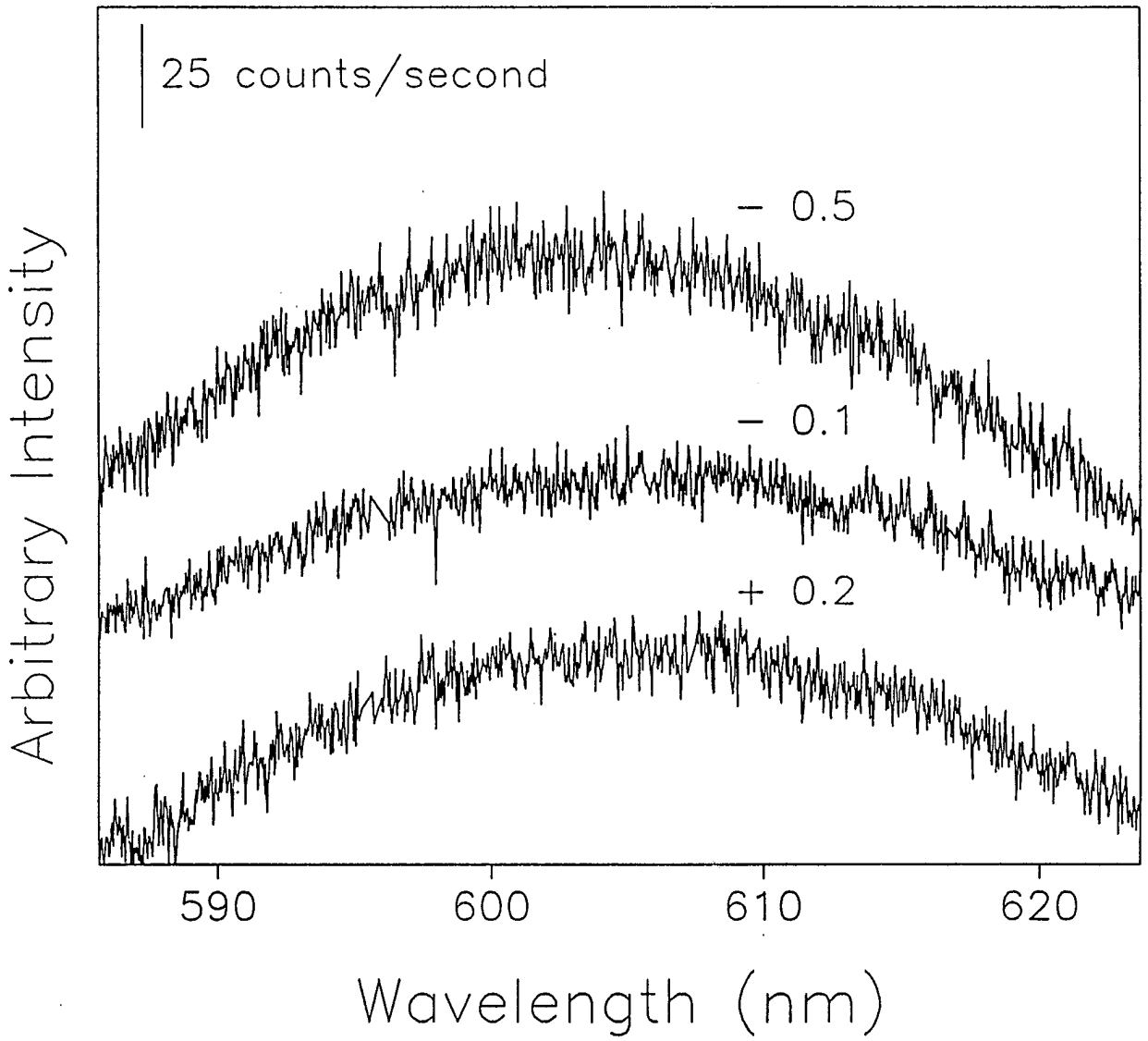
25 counts/second
− 0.5
− 0.1
+ 0.2
Arbitrary Intensity
590
600
610
620
Wavelength (nm)

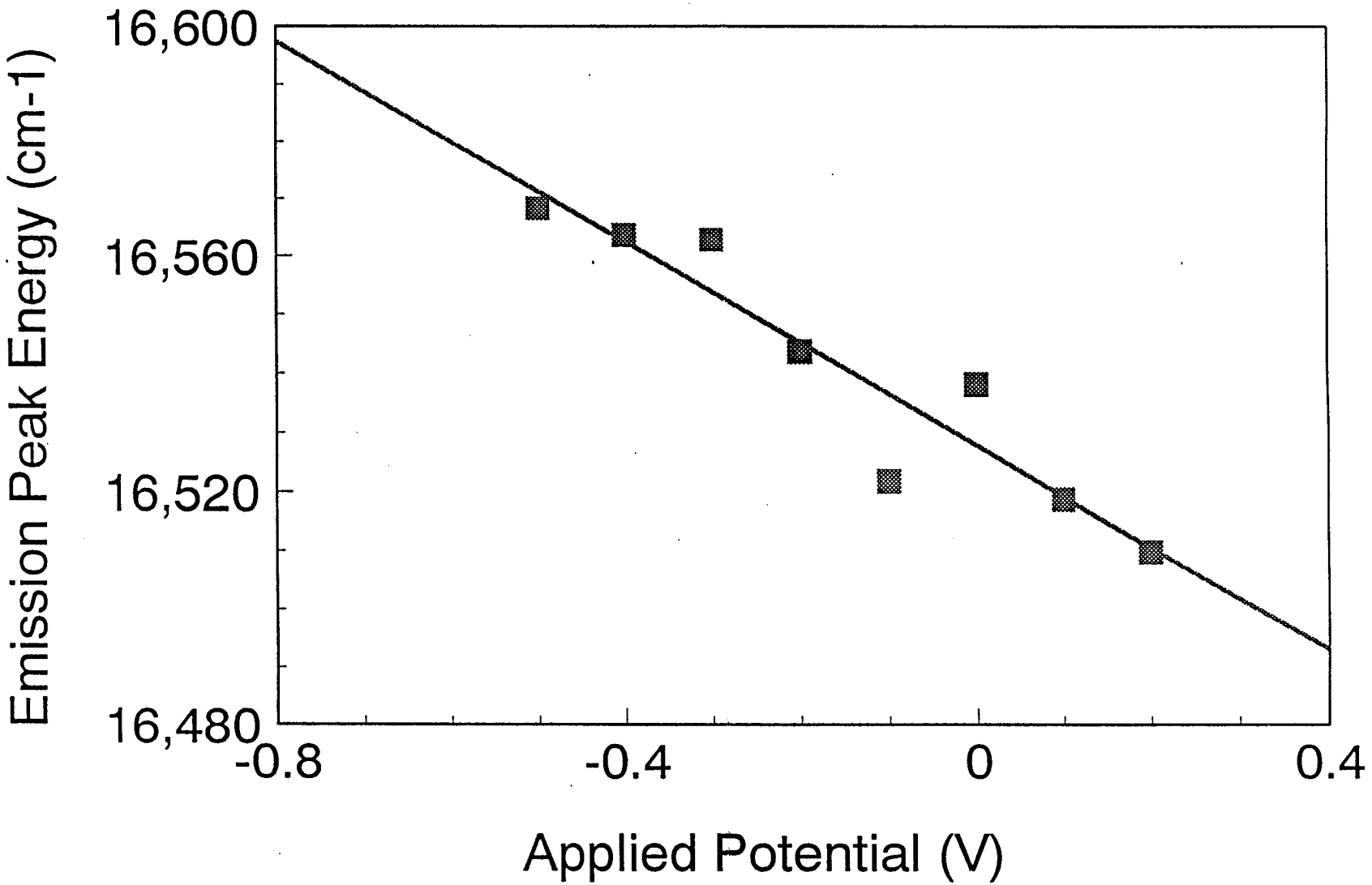
16,600
16,560
16,520
16,480
Emission Peak Energy (cm-1)
-0.8
-0.4
0
0.4
Applied Potential (V)

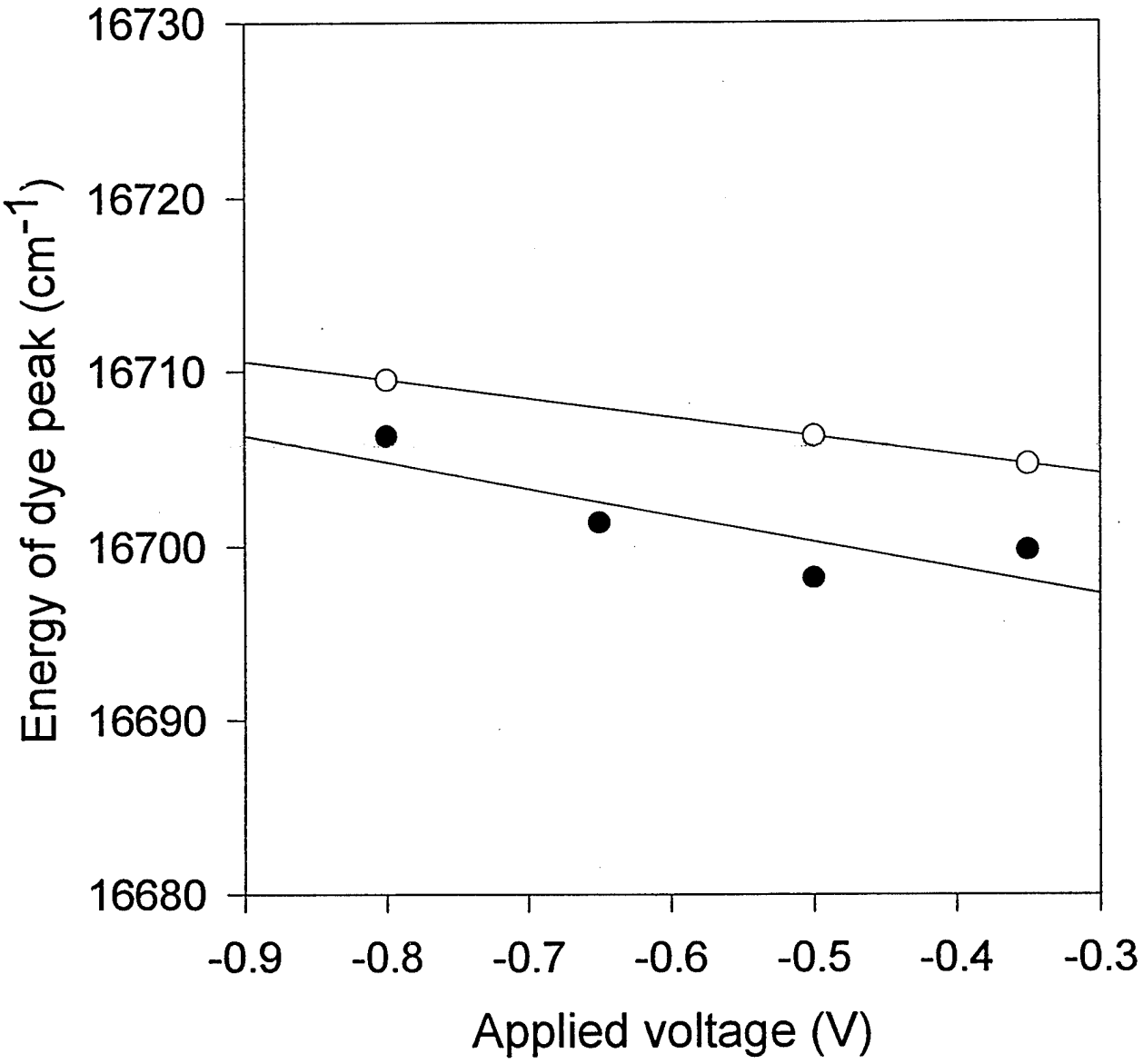
16730
16720
16710
16700
16690
16680
Energy of dye peak (cm-1)
-0.9
-0.8
-0.7
-0.6
-0.5
-0.4
-0.3
Applied voltage (V)

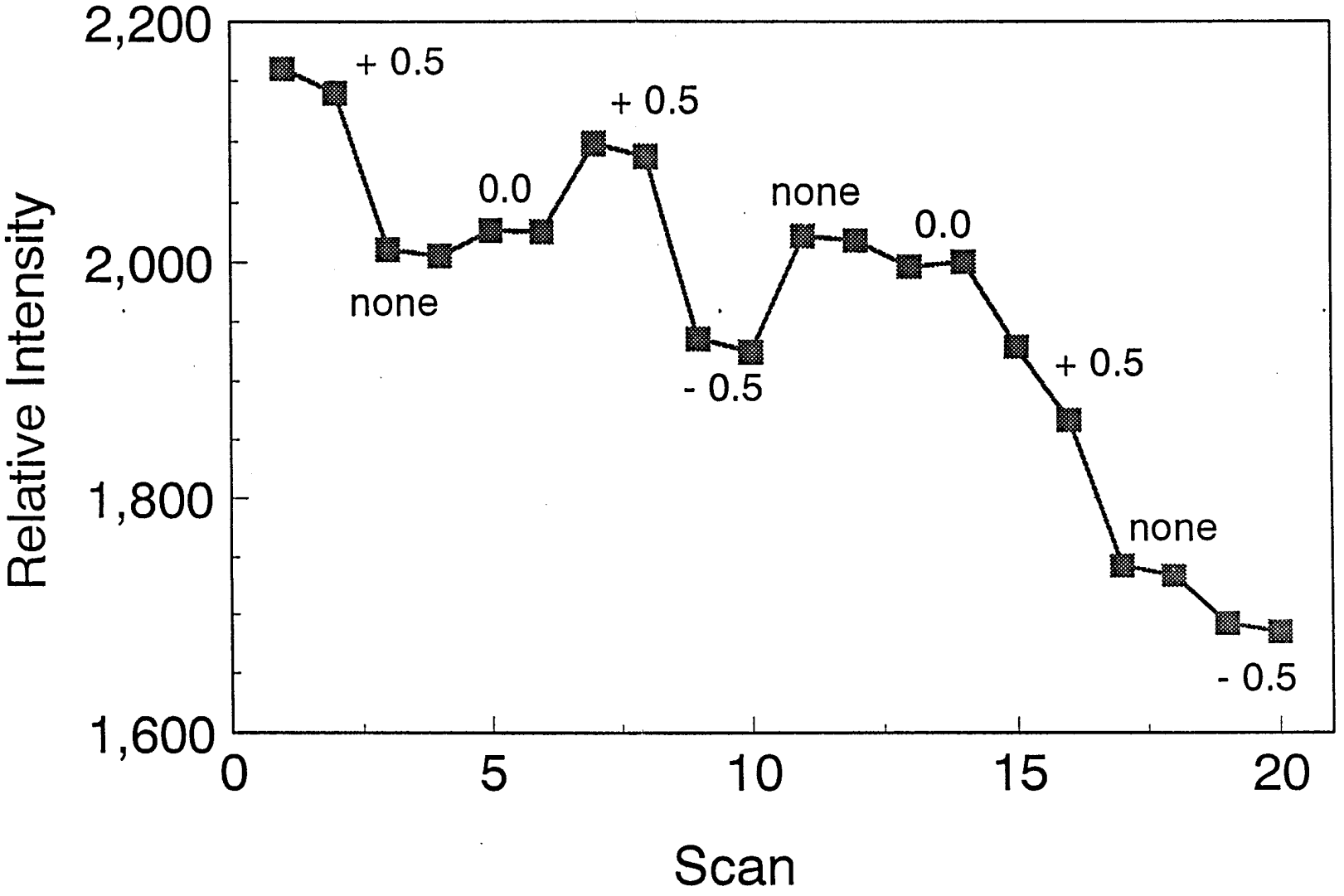
2,200
2,000
1,800
1,600
Relative Intensity
0
5
10
15
20
Scan
+ 0.5
none
0.0
+ 0.5
- 0.5
none
0.0
+ 0.5
none
- 0.5